ORIGINAL RESEARCH

Bioinspired Gold-Silver Bimetallic Nanoparticles from Leaf and Bark Extract of *Simarouba Glauca* and Their Antibacterial Efficacy

Article History
Received: 11-Feb-2024
Revised: 06-Dec-2024
Accepted: 09-Dec-2024
Published: 14-Apr-2025

Natarajan Thangamani[a], Natarajan Bhuvaneshwari[b]*

Abstract: This work reports on using leaf and bark extracts from the *Simarouba glauca* as a natural reducing agent to synthesize gold-silver bimetallic nanoparticles (Ag-Au NPs). The leaf and bark extracts contain phytochemicals such as tannins, flavonoids, and others, confirmed by Fourier transform infrared spectroscopy (FTIR), responsible for the reduction of both Au and Ag ions. The Surface Plasmon Resonance (SPR) bands obtained at 540 and 543 nm, confirmed the formation Au-Ag alloy. The average crystallite size of Au-Ag NPs synthesized using leaf and bark extracts was 29 and 35 nm. TEM images show that the Au-Ag NPs were spherical, square, pentagonal, and hexagonal morphology. The bimetallic nanoparticles were tested against *Staphylococcus aureus, Streptococcus mutans, Bacillus subtilis,* and gram-negative bacteria *Escherichia coli, Proteus vulgaris,* and *Klebsiella Pneumoniae* showed an effective zone of inhibition against the test bacteria. Among the two extracts, the leaf extract was found to be an effective reducing agent to form different shapes of bimetallic nanoparticles. The results indicate that Au-Ag NPs have effective antibacterial activity; hence, these nanoparticles can be used for the development of antibacterial agents.

Keywords: *Simarouba glauca*, Ag-Au Nanoparticles, Antibacterial activity, Green synthesis, Bimetallic Nanoparticles

1. INTRODUCTION

The physical properties, such as surface area, optical, catalytic, chemical and magnetic properties, make the Ag-Au bimetallic nanoparticles unique and distinguishable from Ag and Au nanoparticles (Bawoke and Birhanu, 2023; Thirunavukkarasu and Kuppusamy, 2019). Bimetallic nanoparticles are appropriate for biomedical, biosensors, and wastewater treatment (Arkhipova *et al*., 2024). Many bimetallic nanoparticles have been synthesized using various plant extracts. The advantages of plant extract are naturally available, eco-friendly and harmless to human beings. It is known that different parts of plants, such as leaves, flowers, bark, stem, shoots, and buds are rich in phytochemicals (Chibuye *et al*., 2023). To improve several biomedical applications, plant extracts and their derivatives have been widely employed in place of alternative physical and chemical approaches for the manufacture of bimetallic nanoparticles. It has been postulated that the bioactive components found in the chosen plant act as both capping and reducing agents to stabilize the produced nanoparticles by reducing metal ions (Koushika *et al*., 2024).

Some of the herbs are used as a whole plant extract. Aerial and non-aerial parts of the plants have also been used as natural reducing agents for bimetallic nanoparticle synthesis. The plant extracts contain numerous phytochemicals such as phenolic acids, flavonol, flavonol

a Department of Chemistry, Trinity College for Women, Namakkal – 637002, Tamil Nadu, India.
b Department of Chemistry, Chikkaiah Naicker College, Erode – 638004, Tamil Nadu, India.
* Corresponding Author's Email: drbhuvaneshwari1976@gmail.com

glycoside, carbohydrates, anthocyanins, carboxylic acids, lignins, saponins, and alkaloids. The above-said phytochemicals are freely soluble in water and form homogeneous solutions. Hence, these phytochemicals easily react with silver nitrate and chloroauric acid to form silver and gold nanoparticles. Apart from plant extract, various bacteria and fungi extracts have also been used as reducing agents. This process is simple and fast. This process requires no thermal energy and can be achieved at room temperature (Ashwani *et al*., 2023).

Last five years, many plants such as *Aloe vera*, orange peel, Waste tea leaves, *Persea americana* fruit peel, *Trapa* peel, *Ocimum basilicum (L.)* (Hazarika and Ahmed, 2024), *Pulicaria undulata* (L.), *Abrus precatorius* (Sankareswari *et al*., 2024), *Heliotropium eichwaldi L* (Naila *et al*., 2024), *Callistemon viminalis* (Khan *et al*., 2024), *Thyme plant leaves* extracts (Fujiang *et al*., 2024) have been used for the synthesis of silver-gold bimetallic nanoparticles. In this research, we report on an environmentally friendly way to synthesize Au-Ag bimetallic nanoparticles utilizing leaf and bark extracts of *Simarouba glauca* aqueous. This study is one of the few that has confirmed that Au-Ag phytosynthesized bimetallic nanoparticles, and it is the first report on the use of *Simarouba glauca* for Au-Ag bimetallic nanoparticles. Antimicrobial drugs can be developed using Au-Ag bimetallic nanoparticles.

2. MATERIALS AND METHODS

2.1. Reagents

Chloroauric acid and silver nitrate were purchased from Sigma Aldrich (AR grade with 99.99%), Bangalore. 1×10^{-3} M of silver nitrate and chloroauric acid solutions were prepared using distilled water (stock solutions).

2.2. Extract Preparation

The bark and leaves of *Simarouba glauca* were collected from Kolli Hills, Namakkal District, Tamil Nadu. The bark and leaves were thoroughly washed with tap water followed by distilled water and dried under shade. The powdered bark and leaves, about 50 g were boiled with 100 ml of distilled water and filtered through a muslin cloth followed by Whatmann no.1 filter papers and the filtrate was stored at 5°C in the refrigerator for synthesis.

2.3. Synthesis of Au-Ag NPs

A schematic representation of the synthesis of Au NPs using *Simarouba glauca* leaf extract is shown in Scheme 1. Au-Ag NPs synthesized using leaves extract as follows: the ratios of extract was fixed as 4 mL and the ratio of Ag and Au solution from 0.5 mL to 1.5 mL as follows: 0.5 mL Ag: 1.5 mL Au, 1.0 mL Ag: 1.0 mL Au, and 1.5 mL Ag: 0.5 mL Au. Finally, 1.0 mL Au: 1.0 mL Au was fixed as an optimized concentration. A schematic representation of the synthesis of Au NPs using bark extract is shown in Scheme 2. Au-Ag NPs synthesized using bark extract as follows: the ratios of leaf extract were fixed as 4 mL and the ratio of Ag and Au solution from 0.5 mL to 1.5 mL as follows: 0.5 mL Ag: 1.5 mL Au, 1.0 mL Ag: 1.0 mL Au, and 1.5 mL Ag: 0.5 mL Au. Finally, 1.0 mL Au: 1.0 mL Au was fixed as an optimized concentration. Physical evidence for forming Ag-Au NPs using leaf and bark extracts under the optimized experimental conditions was instantly followed visually by the color changes. Synthesized Ag-Au NPs were stored in the refrigerator at 10°C for three months and were found to be stable.

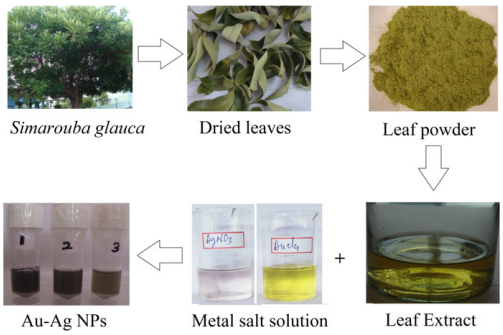

Scheme 1. Synthesis of Au-Ag NPs using leaf extract of Simarouba glauca

Scheme 2. Synthesis of Au-Ag NPs using bark extract of *Simarouba glauca*

https://doi.org/10.37819/nanofab.10.2056

2.4. Characterization Methods

Instrumentation techniques used for the characterization of samples at nano levels. As a result, microscopic techniques like field emission scanning electron microscopy (SEM TESCAN VEGA3 SBH, TSCAN (Floor Model) equipped with EDAX) and transmission electron microscopy (FEI Tecnai G220 S-TWIN, 200 KV, HR-TEM, Spain) were used to observe submicron size materials. Elemental compositions of the samples were determined by energy-dispersive X-ray spectroscopy (EDS or EDAX). A benchtop powder X-ray diffraction instrument (Rigaku miniflex 600, USA) was used to determine the crystal structure of the samples. The UV-visible (SR6 UV-VIS Spectrometers, USA) Spectrophotometer characterization tools are widely used to determine the electronic structures of atoms, ions, and molecules. Fourier transform infrared spectroscopy (Perkin Elmer, Spectrum 2, USA) is generally used to determine the functional group; metal-oxygen bonds present in the samples.

2.5. Antibacterial Activity

The gram positive bacteria used were *Staphylococcus aureus* (*S.aureus*), *Streptococcus mutans (S.mutans)*, and *Bacillus subtilis (B.subtilis)*. Gram negative bacteria used were *Escherichia coli (E. coli)*, *Proteus vulgaris (P. vulgaris)*, and *Klebsiella pneumoniae (K. pneumoniae)*. The Well diffusion method was used to test the samples. About, 10, 20, and 30 µg/ml of the samples were prepared for this test. The test microorganisms were cultivated in the appropriate medium using the spread plate method, containing 10 µl (10 cells/ml) of bacteria grown in nutritional broth for 24 hours. Following solidification, test organism-seeded plates were covered with filter paper wells (5 mm in diameter) that had been impregnated with the extracts. The antibacterial test standard is amoxicillin. For a whole day, the antibacterial assay plates were incubated at 37°C. The inhibitory zone sizes were expressed in millimeters.

The selected bacteria were cultured for 24 hours at 27°C in 20 milliliters of nutrient broth. In particular, the 24-hour cultures were utilized to prepare bacterial lawns on nutrient agar plates. After the bacterial lawn is prepared, a gel-punctured well is created in the solidified agar plates to introduce varying concentrations of Au-Ag NPs prepared using leaves and bark extract. After that, each plate containing a separate bacterium was incubated for 24 hours at 27°C to allow the nanoparticles to diffuse around the well using the diffusion method (Ramesh *et al*., 2019; Santhosh *et al*., 2016). The zone of inhibition was visible in both gram-positive and gram-negative bacteria when the nanoparticles were used. Amoxicillin was used as a positive control. These test results demonstrated the antibacterial activity of synthesized nanoparticles (Kang *et al*., 2019; Yakunin *et al*., 2015).

3. RESULTS AND DISCUSSION

3.1. Synthesis of Au-Ag NPs

Various concentrations of extract 1, 2, 3, and 4 mL of leaf extract were mixed with 2 mL (1.0 mL Ag: 1.0 mL Au) of Au and Ag solutions for the synthesis. Among the four concentrations, 4 mL extract produces a violet color and was further confirmed by a UV-visible spectrometer. The extract concentration was fixed to 4 mL and the ratio of silver chloride and auric chloride was optimized to 0.5 and 1.5 mL. At first, different concentrations and color shifts were used to confirm the creation of Au-Ag NPs. As a result, after adding solutions of silver chloride and chloroauric acid, the pink color of the *Simarouba glauca* aqueous leaf extract turned violet in about 15 minutes. Because of Surface Plasma Resonances (SPR), the intensity of the dark color increased with incubation time. The UV-visible spectrophotometer was used to monitor the formation of Au-Ag NPs at various time intervals. The UV-visible spectrum of Au-Ag NPs is shown in *Simarouba glauca* bark and leaf extracts and was used as a reducing agent without any chemicals. The optical characteristics of Au-Ag NPs can be observed due to the high sensitivity SPR to the size, shape, and composition of the Au-Ag NPs (Meena Kumari *et al*., 2015; Mondal *et al*., 2011).

3.2. UV-Visible Study

Fig.1a shows the UV-vis spectrum of Au-Ag NPs stabilized using leaf extract. The SPR spectrum at 536-540 nm revealed the formation of Au-Ag NPs. However, there is a slight red shift in the SPR band due to the size changes in the particles (Gopalakrishnan *et al*., 2015). The SPR position red-shifted while increasing the concentration of Au NPs. Here, an absorption peak observed for Ag NPs is small and a peak observed at 456 nm. This finding revealed the formation of Au-Ag NPs alloy structure (Csapo *et al*., 2012). Fig. 1b shows the UV-vis spectrum of Au-Ag

NPs. The SPR band revealed that Au-Ag NPs were successfully synthesized using *Simarouba glauca* bark extract. While analyzing using UV-vis spectrum (300-800) nm, the characteristic peak for Au-Ag NPs at 543 nm. The appearance of the peaks at 540 and 543 nm for Au-Ag NPs reveals the presence of a homogenous bimetallic structure rather than a mixture of both Au and Ag NPs (Sahu *et al*., 2020).

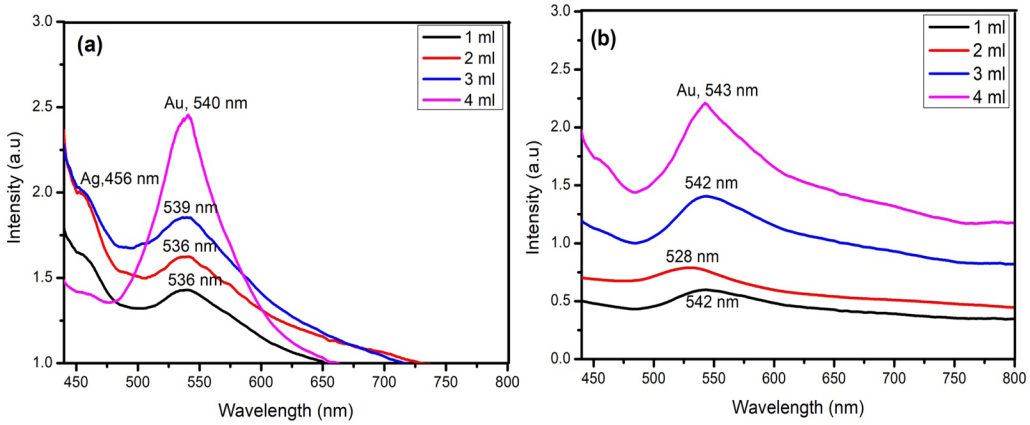

Figure 1. UV-Visible spectra of Au-Ag NPs synthesized using (a) Leaf and (b) Bark extracts of *Simarouba glauca*

3.3. FUNCTIONAL GROUP ANALYSIS

Fig. 2a shows the FTIR spectrum of Au-Ag NPs synthesized using *Simarouba glauca* leaf extract. The bands that were identified in the FTIR spectrum were at 3465, 2085, 1638, and 639 cm^{-1} may be attributed to -OH stretching or another functional group responsible for the C=C, C–OH, C–O, and amine group, respectively (Oladipo *et al*., 2020). These water-soluble biomolecules to play a part in the conversion of Au^{3+} and Ag^{+} to Au^{0} and Ag^{0} (Ibrahim, 2015). However, other bands in 2085 and 1638 cm^{-1} revealed the formation of Au-Ag NPs by phytochemicals present in the extract. A narrow band at 639 cm^{-1} confirmed the presence of Au-Ag NPs. The FTIR spectrum of Au–Ag NPs synthesized using *Simarouba glauca* bark extract is shown in Fig. 2b. The FTIR spectrum of Au-Ag NPs exhibited a broad band at 3448 cm^{-1} and a minor band at 2349 cm^{-1} attributed to stretching vibrations of O–H and C–H groups. The absorption bands at 1639, 1392, 1101, 1026, and 667 cm^{-1} ascribed to C−H deformations, C−C, and C−O stretching vibrations, respectively (Patil *et al*., 2018). The FTIR spectrum confirmed their dual role in the reduction and surface functionalization of Au-Ag NPs (Khademi-Azandehi and Moghaddam, 2015).

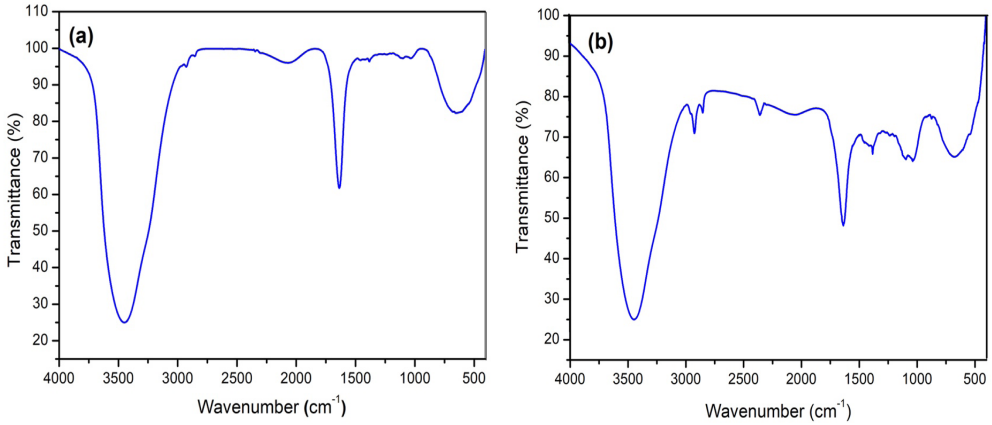

Figure 2. FTIR spectra of Au-Ag NPs synthesized using (a) Leaf and (b) Bark extracts of *Simarouba glauca*

 https://doi.org/10.37819/nanofab.10.2056

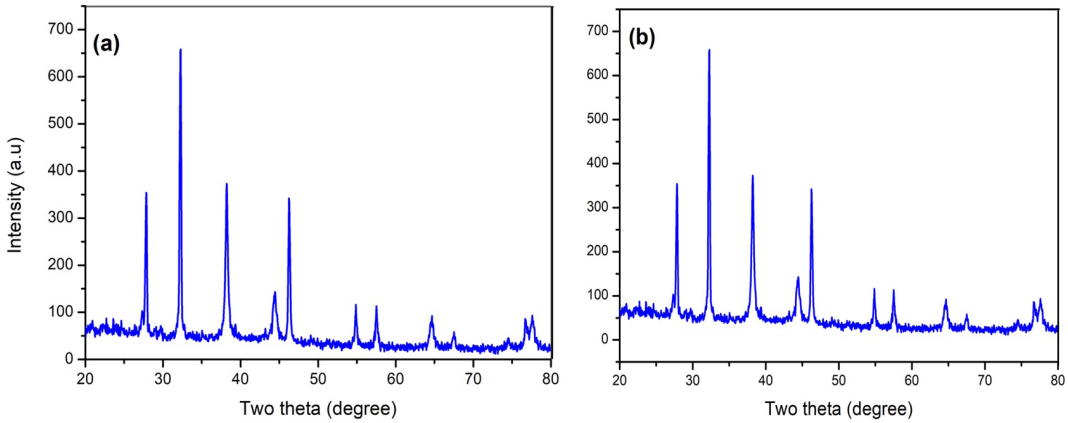

Figure 3. XRD analysis Au-Ag NPs synthesized using (a) Leaf and (b) Bark extracts of *Simarouba glauca*

3.4. Crystalline Phase Analysis

The XRD pattern of the Au-Ag NPs synthesized using leaf extract of *Simarouba glauca* is represented in Fig. 3a**.** The diffraction peaks at 2θ = 38.20, 46.44, 64.68, 77.60, and 78.16° correspond to (111), (200), (220), (311), and (222) planes, respectively (Xia *et al.*, 2013). Apart from the Braggs reflection planes, additional peaks are also found at 2θ values of 27.84, 32.28, 54.88, 57.52, and 67.52, due to the presence of biomolecules (Ibrahim, 2015). The XRD patterns of the Au-Ag NPs synthesized using bark extract are represented in Fig. 3b. The Bragg reflection peaks at 38.16, 46.16, 64.60, and 77.60 could be indexed to (111), (200), (220), (311), and (222) planes of Au-Ag NPs. Apart from the Braggs reflection planes, additional peaks are also found with 2θ values of 27.76, 32.20, 54.72, 57.44, and 67.32 due to the presence of biomolecules. The average crystallite size of the nanoparticles was calculated using Debye–Scherrer's equation (1)

$$D = K\lambda/\beta \cos\theta \qquad (1)$$

The average crystallite size of the nanoparticles was 29 nm. The XRD pattern corresponds with the face-centered cubic (fcc) phase of Au-Ag NPs with (111) plane orientation (Roy *et al.*, 2012). The synthesized bimetallic NPs are highly stable for more than 2 months. The average crystallite size of the nanoparticles was calculated using Scherrer's formula at 29 and 35 nm. The crystalline nature of the Au-Ag NPs is due to an effective reduction of *Simarouba glauca* bark extract, and the synthesized Au-Ag NPs are highly stable for more than 2 months.

3.5. SEM-EDAX Analysis

The structural morphology of green synthesized Au-Ag NPs was identified from the SEM images. FESEM image of Au-Ag NPs synthesized using *Simarouba glauca* leaf extract is shown in Fig. 4a. The SEM images showed clustered or agglomerated spherical particles. Fig. 4(a-ii) revealed the signals for gold and silver atoms and confirmed the formation of Au-Ag NPs. The SEM images of Au-Ag NPs synthesized using *Simarouba glauca* bark extract are displayed in Fig. 4b. The SEM images exhibited clustered and agglomerated spherical particles. However, due to the low resolution of the instrument, only quality limited-quality pictures were obtained for these samples. Fig. 4(b-ii) indicates the signals for gold (29.21%) and silver (70.79%) in Au-Ag NPs with high-intensity peaks. Apart from peaks for Au-Ag NPs, some minor peaks in the spectrum are because of unknown impurities.

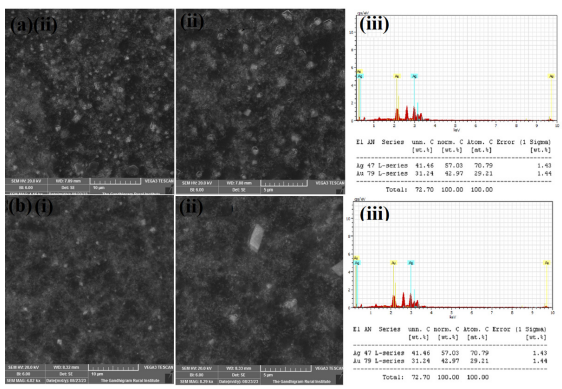

Figure 4. SEM images and EDAX analysis of Au-Ag NPs. In both (a) and (b), (i-ii) represent SEM images and (iii) represents EDAX spectrum

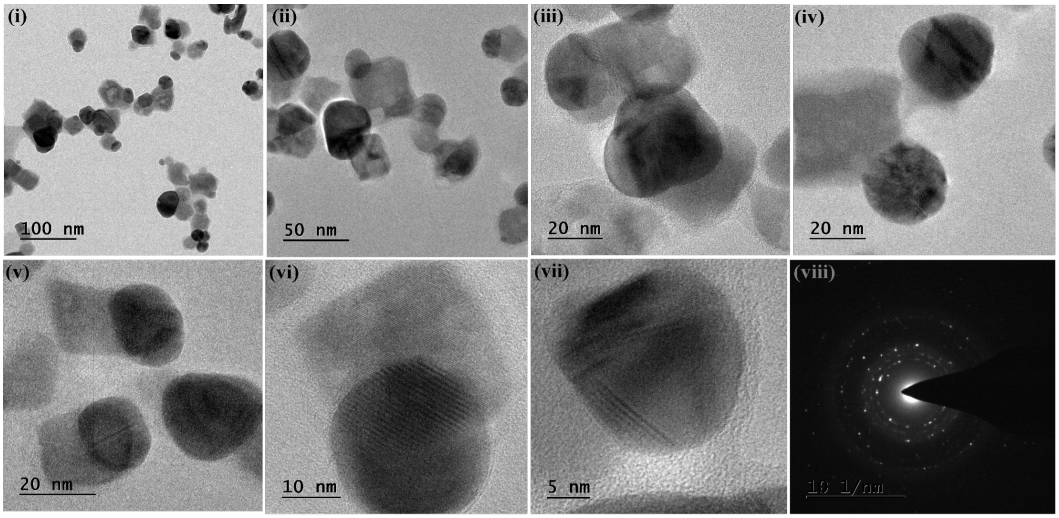

Figure 5. TEM images and SAED pattern of Au-Ag NPs synthesized using Leaf extract. Here, (i-vii) represent TEM images (100 nm-5 nm) taken at different magnifications and (viii) represents SEAD pattern

3.6. TEM Morphology Analysis

The morphology and shape of the bimetallic Au-Ag NPs were obtained from the HR-TEM images. Fig. 5 shows the TEM images of Au-Ag NPs synthesized using *Simarouba glauca* leaf extract. The TEM images exhibited various fascinating shapes like oval, pentagonal, square, and spherical. However, the spherical are visible, as shown in Fig. 5(i-vii). The morphology of bimetallic NPs can be precisely observed at higher magnifications. The particles are predominantly spherical, and aggregation leads to a limited formation of pentagonal and irregularly shaped structures. The particles in Fig. 5(v) show an uneven distribution of particles, suggesting heterogeneous electron density within the volume of particles with an average size of 25 nm representing alloy formation. These results proportionate well with the results obtained from the UV–UV-visible absorption study (Udupa *et al*., 2021). Fig. 6 shows TEM images of Au-Ag NPs synthesized using *Simarouba glauca* bark extract. TEM images exhibited various shapes such as spherical, square, and irregular.

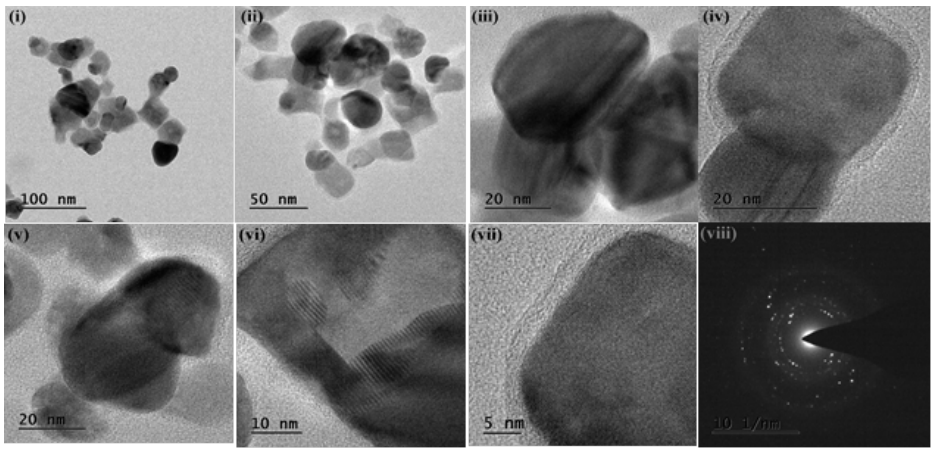

Figure 6. TEM images and SAED pattern of Au-Ag NPs synthesized using Bark extract. Here, (i-vii) represent TEM images (100 nm-5 nm) taken at different magnifications and (viii) represents SEAD pattern

 https://doi.org/10.37819/nanofab.10.2056

3.7. Antibacterial Activity

The antibacterial activity of Au-Ag NPs synthesized using *Simarouba glauca* leaf and bark extracts was tested against three gram-positive bacteria such as *B. subtilis*, *S. aureus*, and *S. mutans*, and three gram-negative bacteria such as *E. coli*, *P. vulgaris*, and *K. pneumoniae*. The zone of inhibition against all the test bacteria is presented in Table 1. Three different concentrations of 10, 20, and 30 µL of Au-Ag NPs solution were used to test the antibacterial activity. Fig. 7 shows the zone of inhibition against different bacteria by leaf extract. The Au-Ag NPs synthesized using 4 mL were tested against these bacteria for antibacterial activity. Three different concentrations of Au-Ag NPs (10, 20, and 30 µl) were tested. Among the test bacteria *S. aureus* (22 mm), *S. mutans* (20 mm), and *Escherichia coli* (22 mm) showed higher zones of inhibition as compared with other bacteria (Table 2). Fig. 8 shows the zone of inhibition against different bacteria by bark extract. The nano-sized Au-Ag NPs easily penetrate the cell walls of the bacteria and inhibit their growth. The positively charged Au and Ag NPs easily get attached to the negatively charged cell wall surface of bacteria. The Au-Ag NPs get attracted and enter easily into the cell wall and release ions into the bacteria to inhibit growth. Then, it produces toxicity to the nucleus of the bacteria, which causes cell death. The decrease in the size of the Au-Ag NPs increases bacterial growth inhibition by freezing the activity of the bacteria. The size and shape of the particles greatly influence the antibacterial activity compared to other morphologies.

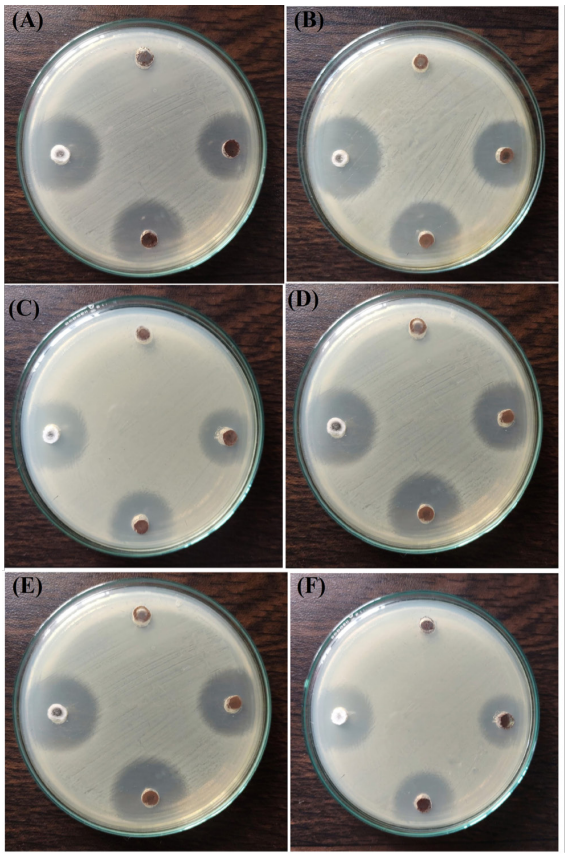

Figure 7. Antibacterial activity of Simarouba glauca leaf extract stabilized Au-Ag NPs. (A) *Staphylococcus aureus*, (B) *Streptococcus mutans,* (C) *Bacillus subtilis,* (D) *Escherichia coli,* (E) *Proteus vulgaris,* and *Klebsiella pneumoniae*

Table 1. Antibacterial activity of Au-Ag NPs synthesized using Leaf extract of *Simarouba glauca*

		Zone of inhibition (mm)			Standard (Amoxicillin)
S.No	Bacteria	10 µl	20 µl	30 µl	5 µl
1	*Staphylococcus aureus*	5	14	18	20
2	*Streptococcus mutans*	5	13	17	20
3	*Bacillus subtilis*	5	10	15	18
4	*Escherichia coli*	5	16	22	24
5	*Proteus vulgaris*	5	16	21	24
6	*Klebsiella pnemoniae*	5	16	19	23

Table 2. Antibacterial activity of Au-Ag NPs synthesized using Bark extract of *Simarouba glauca*

		Zone of inhibition (mm)			
S.No	**Bacteria**	**10 µl**	**20 µl**	**30 µl**	**Standard (Amoxicillin)**
1	*Staphylococcus aureus*	5	18	22	26
2	*Streptococcus mutans*	5	16	20	24
3	*Bacillus subtilis*	5	15	18	22
4	*Escherichia coli*	5	18	22	26
5	*Proteus vulgaris*	5	16	19	22
6	*Klebsiella pnemoniae*	5	15	18	22

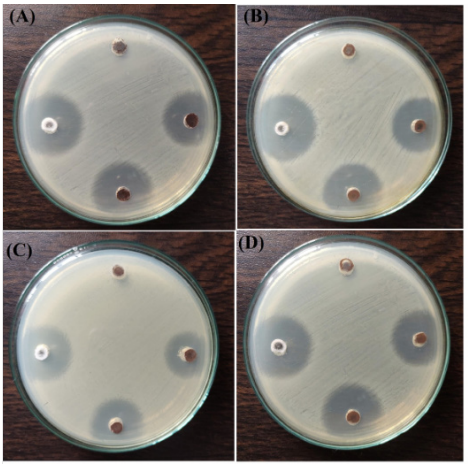

Figure 8. Antibacterial activity of *Simarouba glauca* bark extract stabilized Au-Ag NPs. (A) *Staphylococcus aureus,* (B) *Streptococcus mutans,* (C) *Bacillus subtilis,* (D) *Escherichia coli,* (E) *Proteus vulgaris,* and *Klebsiella pneumoniae*

3.8. Comparison

To understand the capacity of effective reducing capacity, Au-Ag NPs synthesized using leaf was compared with Au-Ag NPs with bark extract. The properties of Au-Ag NPs synthesized using leaf and bark extracts are compared and presented in Table 3. However, small differences were found between them. This variation may be due to the strength of biomolecules present in the leaf extract of *Simarouba glauca.* The GC-MS analysis of *Simarouba glauca* leaf and bark extracts reported to have many phytochemicals such as flavone, oleic acid, phytol, flavones, alkaloids, flavonoids, and other phenolic compounds (Takci *et al*., 2023; Thangamani and Bhuvaneshwari, 2019). The above-mentioned phytochemicals found in the leaf and bark extract might be responsible for reducing Au and Ag ions into Au-Ag bimetallic nanoparticles.

Table 3. Comparison of Au-Ag NPs synthesized using extract of *Simarouba glauca*

S. No	**Parameter**	**Au-Ag NPs**	**Au-Ag NPs**
1	Plant parts	Leaf	Bark
2	Silver nitrate/Auric chloride	1:01	1:01
3	UV absorption	540 nm	543 nm
4	XRD pattern	Fcc	Fcc
5	Average size	24 nm	29 nm
6	EDAX analysis	Au: 63.22%; Ag: 36.78%	Au: 79.79%; Ag: 29.21%
7	TEM morphology	Square, triangle, pentagonal, and dominantly spherical	Square, triangle, and limited spherical particles

4. CONCLUSION

In this work, an aqueous extract of *Simarouba glauca's* leaves and bark was used as a utilized as a reducing agent for the synthesis of Au-Ag NP. It is thought that the phytochemicals in the extract are stabilizing the bimetallic Au-Ag NPs. Water-soluble biomolecules may help the bioreduction of gold and silver ions to produce Au-Ag NPs. The synthesis of bimetallic Au-Ag NPs was demonstrated by spectral characterization and morphological analysis. At λ_{max} 540 and 543 nm. the UV-visible spectrum confirmed the formation of Au-Ag NPs through the SPR band. The SEM analysis revealed the spherical particle size of the synthesized bimetallic NPs. FTIR study confirmed the presence of the functional groups. It was discovered that the Au-Ag NPs had an average size range of 25–29 nm and were primarily spherical. When it comes to bacteria *S. aureus*, *S. mutans*, *B. subtilis*, *E. coli*, *P. vulgaris*, and *K. pneumoniae*, the Au-Ag NPs showed a larger zone of inhibition. Therefore, these Au-Ag NPs can be used for the development of antibacterial agents.

DATA AVAILABILITY STATEMENT

The data used to support the findings of this study are included in the article.

REFERENCES

Bawoke, M., & Birhanu, A. (2023). Nanomaterials: An overview of synthesis, classification, characterization, and applications. *Nano Select*, 4, 486–501. https://doi.org/10.1002/nano.202300038

Thirunavukkarasu, A., & Kuppusamy, V. (2019). Mono- and Bimetallic Au(Core)-Ag (Shell) Nanoparticles Mediated by *Ulva reticulata* Extracts. *ChemistrySelect*, 4, 11009-11014. https://doi.org/10.1002/slct.201903202

Arkhipova, V. I., Mochalova, E. N. & Nikitin, M. P. (2024). Au-based bimetallic nanoparticles: current biomedical applications. *Journal of Nanoparticles Research*, 26, 214. https://doi.org/10.1007/s11051-024-06122-z

Chibuye, B., Singh, S. I., Chimuka, L., & Maseka, K. K. (2023). A review of modern and conventional extraction techniques and their applications for extracting phytochemicals from plants. *Scientific African*, 19, e01585. https://doi.org/10.1016/j.sciaf.2023.e01585

Koushika, S., Vanaraj, S., Mohammed, A. A., Chellasamy, P., & Preethi, K. (2024). Phytoassisted synthesis of biogenic ZnO nanoparticles using *Annona squamosa L*. bark extract: characterization and its application studies. *Green Chemistry Letters and Reviews*, 17, 2024, Article: 2395915. https://doi.org/10.1080/17518253.2024.2395915

Ashwani, K., Nirmal, P., Mukul, K., Anina, J., Vidisha, T., Emel, O., & Fatih, O. (2023). Major Phytochemicals: Recent Advances in Health Benefits and Extraction Method. *Molecules*, 28, 887. https://doi.org/10.3390/molecules28020887

Hazarika, B., & Md. Ahmed, J. L. (2024). Green Synthesis of Au-Ag@TiO_2 Nanocomposite for Photocatalytic Oxidation of Substituted Benzyl Alcohols. *Chemistry Europe*, 9, e202400759. https://doi.org/10.1002/slct.202400759

Sankareswari, M., Amutha, C., Vasantha, V. S., Oh, T. H., Arunpandian, M., & Selvakumar, K. (2024). Biosynthesis of bimetallic Au-Ag nanoparticles using Abrus precatorius seed Extract: Analysis of photocatalytic, cytotoxic, and antibacterial activities. *Inorganic Chemistry Communications*, 169, 113134. https://doi.org/10.1016/j.inoche.2024.113134

Naila, S., Mushtaq, A., Nadia, M., & Omer, K. (2024). Synthesis, Characterization, and Biological Activities of Ag-Au Nanoparticles Using *Heliotropium eichwaldi L*. Extract as a Reducing and Stabilizing Agent. *BioNanoScience*, 14, 4532–4550. https://doi.org/10.1007/s12668-024-01450-9

Khan, S., Rauf, A., Aljohani, A. S. M., Al-Awthan, Y. S., Ahmad, Z., Bahattab, O. S., & Thiruvengadam, M. (2024). Green synthesis of silver and gold nanoparticles in *Callistemon viminalis* extracts and their antimicrobial activities. *Bioprocess and Biosystems Engineering*, 47, 1197–1211. https://doi.org/10.1007/s00449-024-02994-6

Fujiang, Z., Danfeng, H., Guojian, R., & Hossein, Y. (2024). In situ and bio-green synthesis of silver nanoparticles immobilized on zeolite as a recyclable catalyst for the degradation of OPDs. *Scientific Report*, 14, 1143 (2024). https://doi.org/10.1038/s41598-024-51271-9

Ramesh, A., Tamizhdurai, P., Gopinath, S., Sureshkumar, K., Murugan, E., & Shanthi, K. (2019). Facile synthesis of core-shell nanocomposites

Au catalysts towards abatement of environmental pollutant. *Rhodamine B. Heliyon.* 5, e01005. https://doi.org/10.1016/j.heliyon.2018.e01005

Santhosh, S. K., Venugopal, A., & Radhakrishnan, M. C. (2016). Function of Nuclear Factor Kappa B (NF-kB) in Human Diseases-A Review. *South Indian Journal of Biological Science*, 2, 119.

Kang, J., Dietz, M. J., Hughes, K., Xing, M., & Li, B. (2019). Silver nanoparticles present high intracellular and extracellular killing against *Staphylococcus aureus*. *Journal of Antimicrobial Chemotherapy*, 74, 1578–1585.

Yakunin, A. N., Avetisyan, Y. A., & Tuchin, V. V. (2015). Quantification of laser local hyperthermia induced by gold plasmonic nanoparticles. *Journal of Biomedical Optics*, 20, 1–9. https://doi.org/10.1117/1.JBO.20.5.051030

Meena Kumari, M., John, J., & Daizy, P. (2015). Green synthesis and applications of Au-Ag bimetallic nanoparticles. Spectrochimica Acta Part A: Molecular and Biomolecular Spectroscopy, 137, 185–192. https://doi.org/10.1016/j.saa.2014.08.079

Mondal, S., Roy, N., Lascar, R. A., Ismail, S. K., Basu, S., Mandal, D., & Begum, N. A. (2011). Biogenic synthesis of Ag, Au and bimetallic Au/Ag alloy nanoparticles using aqueous extract of mahogany (*Swietenia mahogani* JACQ.) leaves. *Colloids and Surfaces B: Biointerfaces*, 82, 497–504. https://doi.org/10.1016/j.saa.2014.08.079

Gopalakrishnan, R., Loganathan, B. Raghu, K. (2015). Green synthesis of Au–Ag bimetallic nanocomposites using Silybum marianum seed extract and their application as a catalyst. *RSC Advances*, 5, 31691–31699. https://doi.org/10.1039/C5RA03571F

Csapo, E., Oskzo, A., Varga, E., Juhasz, A., Buzas, N., Körösi, L., & Dekany, I. (2012). Catalytic performance of Ag, Au and Ag-Au nanoparticles synthesized by lichen extract. *Colloids and Surfaces A: Physicochemical and Engineering Aspects*, 415 (2012) 281–287. https://doi.org/10.1515/gps-2017-0074

Sahu, S., Sharma, S., Ghosh, K.K. (2020). Novel formation of Au/Ag bimetallic nanoparticles from a mixture of monometallic nanoparticles and their application for the rapid detection of lead in onion samples. *New Journal of Chemistry*, 44, 15010–15017. https://doi.org/10.1039/D0NJ02994G

Oladipo, A. O., Iku, S. I., Ntwasa, M., Nkambule, T. T. I., Mamba, B. B., & Msagati, T. A. (2015). Doxorubicin conjugated hydrophilic AuPt bimetallic nanoparticles fabricated from Phragmites australis: Characterization and cytotoxic activity against human cancer cells. *Journal of Drug Delivery Science and Technology*, 57 (2020) 101749. https://doi.org/10.1016/j.jddst.2020.101749

Ibrahim, H. M. M. (2015). Green synthesis and characterization of silver nanoparticles using banana peel extract and their antimicrobial activity against representative microorganisms. *Journal of Radiation Research Applied Science*, 8 (2015) 265–275. http://dx.doi.org/10.1016/j.jrras.2015.01.007

Patil, M. P., Jin, X., Simeon, N. C., Palma, J., Kim, D., Ngabire, D., & Kim, G. D. (2018). Anticancer activity of *Sasa borealis* leaf extract-mediated gold nanoparticles. *Artificial Cells, Nanomedicine, and Biotechnology*, 46, 82–88.

Khademi-Azandehi, P., & Moghaddam, J. (2015). Green synthesis, characterization and physiological stability of gold nanoparticles from *Stachys lavandulifolia* Vahl extract. *Particuology*, 19, 22–26. https://doi.org/10.1016/j.partic.2014.04.007

Xia, B., He, F., & Li, L. (2013). Preparation of Bimetallic Nanoparticles Using a Facile Green Synthesis Method and Their Application. *Langmuir*, 29, 4901–7. https://doi.org/10.1021/la400355u

Roy, N., Alam, M. N., Mondal, S., Ismail, S. K., Laskar, R. A., Das, S., & Begum, N. A. (2012). Exploring Indian Rosewood as a promising biogenic tool for the synthesis of metal nanoparticles with tailor-made morphologies, *Process Biochemistry*, 47, 2012, 1371–1380. https://doi.org/10.1016/j.procbio.2012.05.009

Udupa, A. V., Gowda, B., Kumarswammy, B. E., & Shivanna, M. B. (2021). The antimicrobial and antioxidant property, GC–MS analysis of non-edible oil-seed cakes of neem, madhuca, and simarouba. *Bulletin of the National Research Centre*, 45, 41. https://doi.org/10.1186/s42269-021-00498-x

Takcı, D. K., Ozdenefe, M. S., & Genc, S. (2023). Green synthesis of silver nanoparticles with an antibacterial activity using Salvia officinalis aqueous

extract. *Journal of Crystal Growth*, 614, 127239. https://doi.org/10.1016/j.jcrysgro.2023.127239. https://doi.org/10.1186/2193-1801-2-28

Thangamani, N., & Bhuvaneshwari, N. (2019). Green synthesis of gold nanoparticles using Simarouba glauca leaf extract and their biological activity of micro-organism. *Chemistry Physics Letters*, 732, 136587. https://doi.org/10.1016/j.cplett.2019.07.015